# Laser spectroscopy of the HgCd exciplex

J. Supronowicz, D. Petro, J. B. Atkinson, and L. Krause
*Department of Physics, University of Windsor, Windsor, Ontario, Canada N9B 3P4*
(Received 21 December 1993)

Fluorescence and excitation spectra of HgCd were studied using pump-and-probe methods of laser spectroscopy with time resolution. A Hg-Cd vapor mixture, contained in a sealed quartz cell at 700 K, was irradiated by consecutive pump and probe dye-laser pulses. The pump radiation produced a population of Cd $5\,^3P_1$ atoms whose three-body collisions with Hg atoms resulted in the formation of HgCd excimers in the $A0^-$, $A0^+$, and $A1$ states, correlated with the Cd $5\,^3P$+Hg $6\,^1S$ manifold, which decayed, emitting a previously reported 4600-Å fluorescence continuum. The probe pulses, delayed by 450 ns, excited the excimers to the higher-lying $C0^+$ (Cd $5\,^1P_1$+Hg $6\,^1S_0$) state, which decayed to the repulsive $X0^+$ ground state, emitting fluorescence in the 2400–2650-Å region. We also observed a bound-bound excitation spectrum in the 5800–7100-Å region. A study of the time evolution of the excimer fluorescence yielded an approximate value for the three-body rate coefficient for HgCd formation, and an analysis of the spectra produced spectroscopic constants for the states involved in the transitions.

PACS number(s): 33.20.−t, 33.50.Dq

## I. INTRODUCTION

The spectroscopy of the HgCd excimer is virtually unknown. Some 10–15 years ago there were several reports of investigations probing the kinetics of HgCd excimer formation and its potential suitability as a laser medium [1–6]. Various methods were used to produce the HgCd excimer, including optical excitation of the Cd $5^3P_1 \leftarrow 5^1S_0$ transition with 3261-Å radiation [1,6], pumping the Hg-Cd vapor mixture with the 2660-Å fourth harmonic of a Nd:YAG (neodymium-doped yttrium-aluminum-garnet) laser [4] or with the filtered output of a Xe flash lamp [3] to induce formation of HgCd by photoassociation, and electron impact [5]. The most extensive kinetic studies were carried out by McGeoch and co-workers [1–4], who suggested the existence of two low-lying HgCd excimer states that emitted blue fluorescence in their decay to the ground state, but with different decay times. The authors did not attempt to identify these states but merely labeled them "CdHg*(a)" and "CdHg*(b)."

Like the other excimers consisting of atoms belonging to the 2b group of the periodic table, HgCd exhibits a repulsive ground-state potential-energy (PE) curve, except for a weak van der Waals minimum at a relatively large equilibrium internuclear separation ($r_e$) with a depth of a few hundred wave numbers. The molecule should be expected to possess a variety of strongly bound states with PE well depths reaching $10^4$ cm$^{-1}$, similar to those that have been observed in HgZn [7]. In addition to the previously reported blue (4600-Å) fluorescence band, we excited such a higher-lying bound state using the pump-and-probe method and recorded the resulting bound-bound excitation spectrum as well as the bound-free fluorescence spectrum, both of which we describe in this article.

## II. PE DIAGRAM FOR HgCd

Figure 1 shows a semiquantitative PE diagram for HgCd [8] which was derived from the calculated HgZn curves [7]. The Cd and Zn atoms have very similar electronic structures which, in the ground state, include two valence electrons that have the same orbital quantum number $l=0$. The HgCd curves were produced by using the calculated curves for HgZn and matching them at large internuclear distances to the asymptotic states of HgCd. The symmetry of these states remains the same but they are asymptotic to different atomic energy levels. Whenever possible, we kept the same depth of PE wells, except when avoided crossings did not permit this, and then we changed the depth of the wells to obtain the best qualitative picture of the avoided crossing region.

One of the major differences between the potential curves of HgZn and HgCd arises from the fact that the atomic state $6\,^3P_2$ of Hg lies well below the $4\,^1P_1$ state of Zn but the $6\,^3P_2$ state in Hg lies above the $5^1P_1$ state of Cd. This causes a change in the sequence of the atomic asymptotic states to which the molecular states merge at large internuclear distances $r$. Thus Hg($6\,^3P_2$)+Zn($4\,^1S_0$) lies below Hg($6\,^1S_0$)+Zn($4\,^1P_1$) [7] but, as may be seen in Fig. 1, in HgCd the order is opposite and Hg($6\,^1S_0$)+Cd($5\,^1P_1$) lies below Hg($6\,^3P_2$)+Cd($5\,^1S_0$). Similarly, the two states $D1$ and $E1$ merge at large $r$ into Hg($6\,^1S_0$)+Cd($5\,^1P_1$) and Hg($6\,^3P_2$)+Cd($5\,^1S_0$), respectively, but in HgZn, the $D1$ and $E1$ molecular states are associated with Hg($6\,^3P_2$)+Zn($4\,^1S_0$) and Hg($6\,^1S_0$)+Zn($4\,^1P_1$), respectively [7]. The curves have to be drawn as shown in Fig. 1 to avoid a crossing between $\Omega=1$ curves of the same symmetry. The $C0^+$ state, which asymptotically merges with Hg($6\,^1S_0$)+Cd($5\,^1P_1$), is also shallower than the analogous state in HgZn, to avoid a crossing with the

 

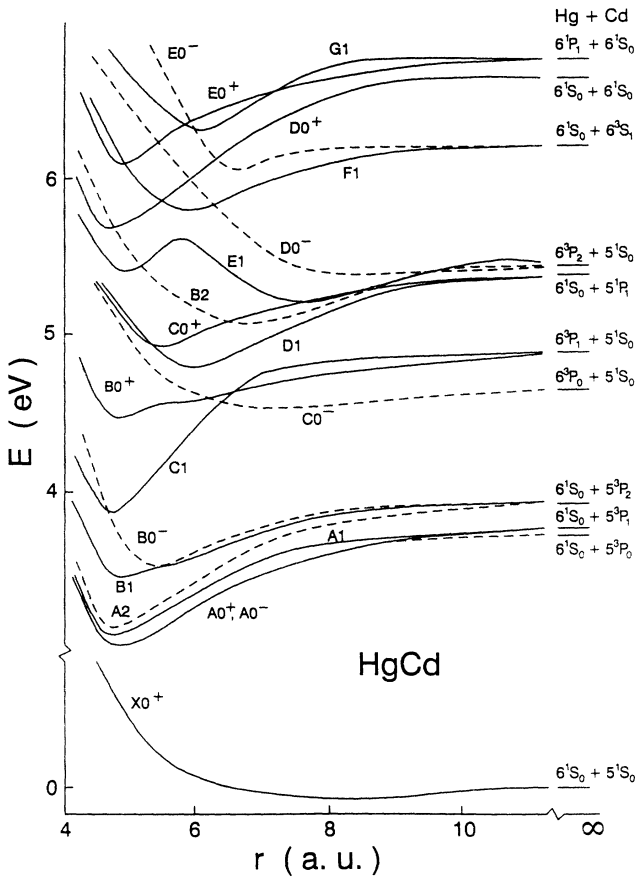


FIG. 1. A potential-energy diagram for the HgCd molecule drawn according to Hund's case (c) coupling. The dashed lines represent the states which cannot decay to the repulsive ground state because of selection rules.

$B0^+$ state, which arises from the $Hg(6\,^3P_1)+Cd(5\,^1S_0)$ asymptotic state. The reason for this is that the energy gap between the $Cd(5\,^1P_1)$ and $Hg(6\,^3P_1)$ states is smaller than the gap between $Zn(4\,^1P_1)$ and $Hg(6\,^3P_1)$.

The depth of the potential well for the $X0^+$ ground state of HgCd was estimated by the use of the expression $\epsilon_{12}=\sqrt{\epsilon_1\epsilon_2}$ [9], where $\epsilon_1$ and $\epsilon_2$ are the well depths of the homonuclear potentials and $\epsilon_{12}$ is the estimated value of the well depth for the appropriate heteronuclear molecule. Taking $\epsilon_1=0.043$ eV for the ground state of $Hg_2$ [10] and $\epsilon_2=0.040$ eV for $Cd_2$ [11], we obtain $\epsilon_{12}=0.042$ eV for the ground state of HgCd.

The potential-energy curves of HgZn were calculated using the "configuration interaction by perturbation with multiconfigurational zeroth-order wave functions selected by iteration" (CIPSI) method [12]. Only the four valence electrons were explicitly involved. The two cores, $Hg^{2+}$ and $Zn^{2+}$, were treated in a similar way, despite the fact that all the electrons of Zn were taken into account at the self-consistent field (SCF) level whereas a pseudopotential was used for Hg. In the CIPSI method the effect of configuration interaction was calculated by a Rayleigh-Schrödinger perturbation expansion, starting from a multiconfigurational wave function. In addition, the interatomic correlations were estimated by a semiempirical procedure. The fine structure of the calculated molecular states was taken into account by the use of the atomic spin-orbit coupling matrices given by Hay, Dunning and Raffenetti [13]. This procedure was carried out for the lowest molecular state arising from the triplet atomic states. The assumption was made that the spin-orbit parameters did not vary with internuclear distance.

## III. EXPERIMENTAL DETAILS

The arrangement of the apparatus used to record the spectra is shown in Fig. 2. A cylindrical quartz cell, 10 cm long and 2.5 cm in diameter, was charged with redistilled Cd (120 mg) and Hg (460 mg). Hg and Cd form an amalgam and the resulting equilibrium partial Cd and Hg vapor pressures above the liquid phase may be derived from the expression [14,3]

$$\frac{P_a}{P_a^0}=X_a\exp\left[-\frac{C}{T}(1-X_a)^2\right], \tag{1}$$

where $P_a^0$ is the equilibrium vapor pressure over the pure metal $a$, $X_a=N_a/(N_a+N_b)$ is the mole fraction of $a$ in the liquid, and $C=1000$ K for Cd-Hg amalgams. The tendency resulting from an excess of metal $b$ over $a$ in the liquid phase is the strong suppression of the partial pressure of $a$, in comparison with its equilibrium vapor pressure over the pure (liquid) metal $a$ at the same temperature.

The quartz cell had a 15-cm-long side arm protruding downwards and was placed in an electrically heated oven that had separate compartments and temperature controls for the main body of the cell and the side arm. During the experiments the body of the cell was maintained at 710 K and the side arm at 620 K. We estimated that under these conditions the partial pressure of Cd was near 0.045 torr, which corresponded to an atomic number density of $6.12\times10^{14}$ cm$^{-3}$, and the partial pressure of Hg was about 335 torr ($4.56\times10^{18}$ cm$^{-3}$). At these densities we were able to excite fluorescence spectra of adequate intensity and acceptable signal-to-noise (S/N) ratio. The vapor mixture in the cell was irradiated with two consecutive laser pulses parallel to the cell axis and antiparallel to each other. The first (pump) pulse was the frequency-doubled output of a dye laser which was excited with the second harmonic of a Nd:YAG laser. This radiation of wavelength 3261 Å produced a population of Cd $5\,^3P_1$ atoms; the full width at half-maximum (FWHM) of the pulse was 8–10 ns and its average energy was near 0.1 mJ. The second (probe) pulse, which was of comparable FWHM and was delayed by about 450 ns relative to the pump pulse, was generated by a $N_2$-laser-pumped dye laser which could be scanned in constant wavelength increments. Several laser dyes were used to cover the 5500–7200-Å excitation region which was probed in the course of the experiments. The repetition rates for both lasers were set at 10 Hz. Both beams were focused to a diameter of about 1 mm and were overlapped in the region of observation. The resulting

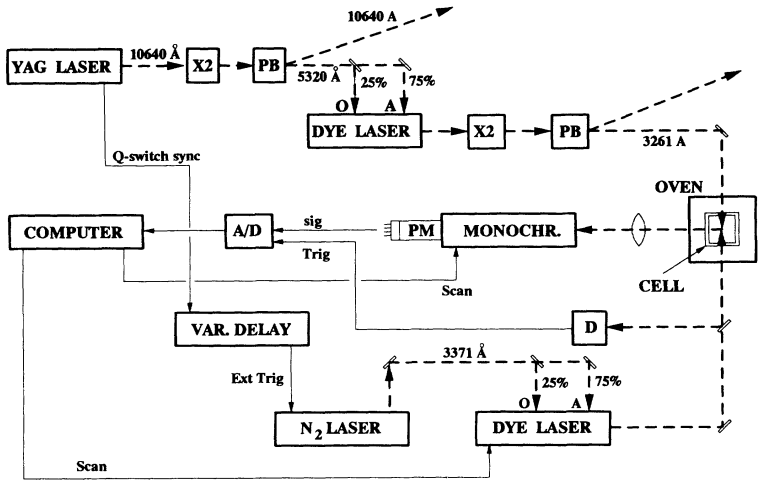


FIG. 2. A schematic diagram of the apparatus. PB, Pellin-Broca prism; D, photodiode; M, monochromator; A/D, digitizing oscilloscope; PM is a photomultiplier tube.

fluorescence was observed at right angles to the beams, resolved with a monochromator, and detected with a photomultiplier. The photomultiplier signal was registered with a transient digitizer (Hewlett-Packard model HP 54111 D digitizing oscilloscope) and summed in a microcomputer that also controlled the scanning of the monochromator and the probe dye laser. In the visible region we used a 0.85-m SPEX model 1402 double monochromator, fitted with an RCA model 31034 photomultiplier tube and, in the ultraviolet, 0.25-m and 0.64-m Jobin-Yvon (JY) monochromators with Peltier-cooled EMI 9816QB photomultipliers.

With this apparatus we recorded the fluorescence and excitation spectra and studied the time evolution of the fluorescence. To record the fluorescence spectrum resulting from only pump or pump-and-probe excitation, we scanned the fluorescence with the monochromator in small wavelength increments while keeping the laser(s) tuned to a particular wavelength or wavelengths. The resulting signal, corresponding to the wavelength increment, was time integrated, summed over 10 or 20 laser pulses (or pump-and-probe pulse pairs), and stored in the computer memory, and the monochromator was then advanced to the next wavelength setting. The procedure followed in recording the excitation spectrum was similar, except that the monochromator was set at a fixed wavelength while the probe laser was scanned across the excitation spectrum. In both cases the scans were repeated several times until the signal-averaging procedure yielded an acceptable S/N ratio. Since in the pump-and-probe experiments the resulting fluorescence was quite short-lived, the transient digitizer was set to record the signal produced during 25 ns following the probe pulse, because this time span was found to contain virtually 100% of the emitted fluorescence. The spectrum of the longer-lived fluorescence excited with only the pump pulses was collected over a time interval of about 20 $\mu$s, which was equivalent to several mean persistence times of the fluorescence emission.

The time-evolution experiments encompassed studies of the 4600-Å emission excited with the pump radiation, as well as the fluorescence produced by pump-and-probe excitation. When studying the 4600-Å emission, the time evolution of the signal following each pump pulse was recorded with the transient digitizer and averaged over several hours on the computer, with a time resolution that could be varied down to 1 ns. When investigating the variation of the intensity of the fluorescence, produced by pump-and-probe excitation, with time delay between the pump and probe pulses, both the monochromator and probe laser were set on predetermined wavelengths and the pump-probe delay was varied using a computer-controlled (in-house built) delay generator which had a 5-ns resolution. In these experiments we also used signal averaging to improve the S/N ratio.

## IV. RESULTS AND DISCUSSION

### A. Kinetics of HgCd formation

Figure 3 shows a trace of the persistent fluorescence continuum in the 3800–5500-Å region, produced by pump-laser excitation. The intensity profile was corrected for the spectral response of the SPEX monochromator and the photomultiplier, which were together calibrated against a spectral irradiance standard.[1] The profile, which includes Hg and Cd atomic lines probably resulting from multiphoton excitation, is symmetric about the 4600-Å maximum and is unstructured.

The results of previous experiments on the HgZn exciplex [15–17] indicated that the exciplex is formed according to the mechanism

$$\mathrm{Zn}(4\,^3P)+2\mathrm{Hg}(6\,^1S_0)\rightarrow\mathrm{HgZn}^*+\mathrm{Hg}(6\,^1S_0)\ . \qquad (2)$$

We suggest that a similar collisional mechanism governs the formation of the HgCd exciplex:

$$\mathrm{Cd}(5\,^3P_{0,1,2})+2\mathrm{Hg}(6\,^1S_0)\rightarrow\mathrm{HgCd}^*+\mathrm{Hg}(6\,^1S_0)\ . \qquad (3)$$

This contention is supported by the results of our experi-

[1] A 200-W quartz halogen lamp was used, calibrated by the Canadian National Research Council Laboratories.

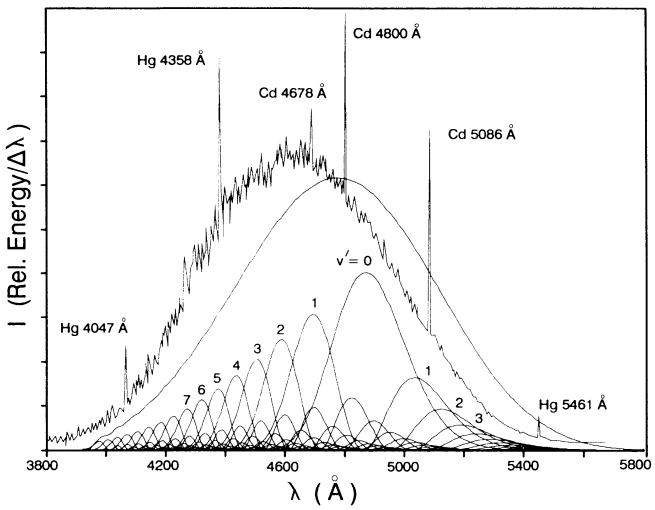


FIG. 3. A trace of the fluorescence continuum in the 3800–5500-Å region, produced by 3261-Å laser excitation. The intensity $I$ is given in arbitrary units of intensity per λ interval. The curves under the trace represent the simulated emission intensities due to the first 16 vibrational levels of the $A0^+$ state, and their sum (see Sec. IV).

ments on the kinetics of the collisional interactions of Cd atoms in $5\,^3P_J$ fine-structure states with ground-state Hg atoms [18], and from observations of the time behavior of the HgCd molecular fluorescence and Cd atomic resonance fluorescence following pump-pulse irradiation. Figure 4 shows the time evolution of the 4600-Å HgCd band over a 20-μs time span and Fig. 5 shows the time evolution of the 3261-Å Cd resonance line, which represents the time behavior of the Cd $5\,^3P_1$ population. The latter can be fitted to a sum of three exponential (decaying) terms since there is collisional mixing among the Cd $^3P_J$ states. The three decay rates correspond (approximately) to the rates of transfer from the $5\,^3P_1$ state to each of the $5\,^3P_0$ and $5\,^3P_2$ states, and to the decay of the

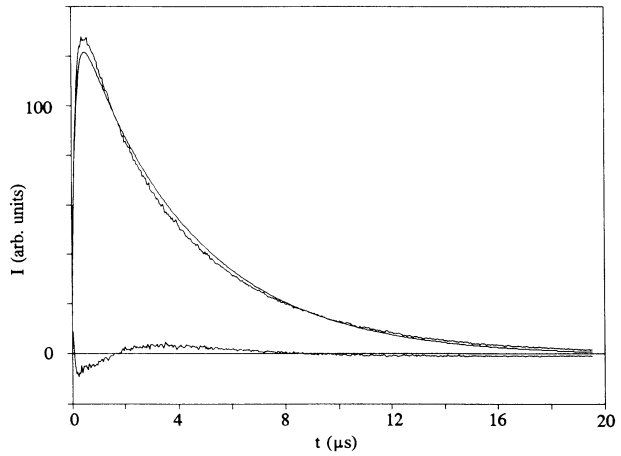


FIG. 4. Time evolution of the 4600-Å HgCd fluorescence band. The smooth curve shows the best fit of Eq. (5); the residual is also shown.

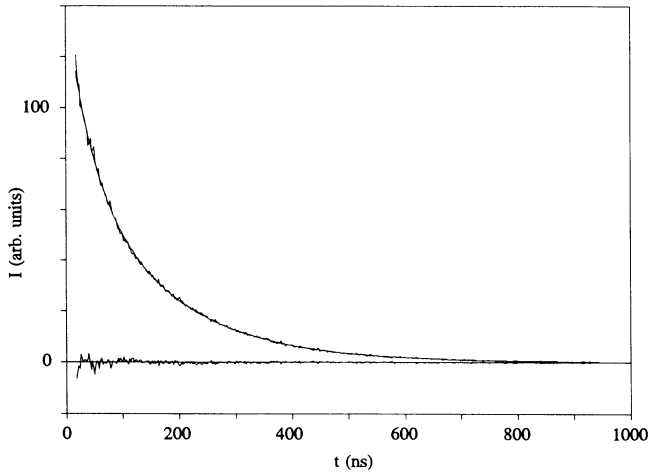


FIG. 5. Time evolution of the 3261-Å atomic fluorescence following the pump-laser pulse, showing the experimental data, the best fit of Eq. (6), and the residual.

whole $^3P$ manifold. The latter results from the fluorescent emission at 3261 Å from the $5\,^3P_1$ state, quenching by impurities, and HgCd formation whose rate is quadratic in Hg($6\,^1S_0$) atomic number density.

The 4600-Å fluorescence continuum is most likely emitted in the decay of the $A0^+$ and/or $A1$ states, both of which can combine with the $X0^+$ ground state. The $B1$ state, which is the next lowest state that could also decay radiatively to the $X0^+$ state, would have a much smaller population at the temperature of the vapor cell, assuming that the populations are thermalized. The $A0^+$, $A0^-$, and $A1$ states also constitute the long-lived "reservoir" states from which further excitation is effected by the probe-laser pulses. On the basis of our previous experience with the $Hg_2$ and HgZn systems [7,19], we believe that the $A0^+$, $A0^-$, and $A1$ states undergo rapid thermalization due to the very frequent two-body collisions, and that their relative populations are determined by the Boltzmann law.

If the formation of the HgCd exciplex is correctly described by Eq. (3), and if the depopulation rate for the HgCd excited states depends linearly on the excited-state population, then the time evolution of the 4600-Å fluorescence band can be described by the equation

$$dN/dt=\Gamma_a N_a-\Gamma N\ , \tag{4}$$

where $N$ is the combined population density of the HgCd reservoir states ($A0^+$, $A0^-$, $A1$), $N_a$ is the population density of the Cd($5\,^3P$) manifold, $\Gamma_a$ is the rate constant for the formation of HgCd, and $\Gamma$ is the decay rate constant for the HgCd reservoir states whose depopulation is mainly due to radiative decay by fluorescence emission. With the initial condition $N(t=0)=0$, the solution of Eq. (4) is

$$N(t)=\sum_{i=1}^{3}[\Gamma_a N_{0i}/(\beta_i-\Gamma)][\exp(-\Gamma t)-\exp(-\beta_i t)]\ , \tag{5}$$

where we have assumed that

$$N_a = \sum_{i=1}^{3} N_{0i}\exp(-\exp\beta_i t) \tag{6}$$

to include the three exponential terms in the decay of the $5\,^3P$ manifold. The values of $1/\beta_i$ were 160, 42, and 2 ns, respectively, with the slowest decay ($1/\beta = 160$ ns) corresponding to the decay of the whole $5\,^3P$ manifold. Figure 4 contains the plot of Eq. (5) with only one value of the atomic decay constants $\beta$ included, corresponding to the slowest decay in Fig. 5. No improvement in fit could be obtained by including the intermediate and/or fast $\beta_i$ terms. Figure 6 shows the rise of the molecular fluorescence, corresponding to the first 1 $\mu$s in Fig. 4, and it may be seen that the rise time is approximately 160 ns, matching the slowest decay rate of the atomic fluorescence. The fit of Eq. (5) to the experimental data in Fig. 4 was improved by including in Eq. (4) a term representing bimolecular quenching [17], which results from the collision of two HgCd* molecules of which one is quenched to the dissociative ground state. The time evolution now becomes

$$dN/dt = \Gamma_a N_a - \Gamma N - kN^2 , \tag{7}$$

where $k$ is the bimolecular quenching rate constant.

Equation (7) was solved for a single $\beta$ term in Eq. (6), by writing $N = (du/dt)/ku$ and solving a second-order differential equation for $u$, whose solution is

$$ku = 1 - \exp(-\Gamma t)\left[\sum_{m=0}^{\infty} a_m \exp(-m\beta t)\right] + \left[\sum_{m=1}^{\infty} b_m \exp(-m\beta t)\right] , \tag{8}$$

where

$$\begin{aligned} a_m &= [k\Gamma_a N_0/m\beta(m\beta+\Gamma)]a_{m-1} , \\ b_m &= [k\Gamma_a N_0/m\beta(m\beta-\Gamma)]b_{m-1} , \\ b_1 &= k\Gamma_a N_0/\beta(\beta-\Gamma) . \end{aligned} \tag{9}$$

$a_0$ is determined by the initial value of $N$ at $t=0$. If $k\Gamma_a N_0/\beta^2 < 1$, the terms in the sums of Eq. (8) are negligible for $m > 3$. Figure 7 shows the best fit of Eq. (8) to the experimental data shown in Fig. 4, with the scale of the residuals magnified by a factor of 10. The value of $kN_{\max}/\Gamma$ corresponding to the best fit is 0.462, but an absolute determination of $N_{\max}$ would be required to obtain a value of $k$.

Figures 8–10 show the time evolutions of the molecular and atomic fluorescence at a lower Hg density of $1.67\times10^{18}$ cm$^{-3}$. At the lower density, the values of $1/\beta$ were 1400, 76, and 10 ns, respectively. As would be expected, the fluorescence is less intense than at higher Hg densities, which manifests itself by a decrease in the S/N ratio and in the $kN_{\max}/\Gamma$ value, which becomes $2.6\times10^{-3}$ as the result of a decrease in $N_{\max}$. The slowest decay rate of the atomic fluorescence matches the value of $\beta$ in Eq. (5). Although the decay of the molecular fluorescence appears to be slower in Fig. 8 than in Fig. 7, the values of $\Gamma$ at high and low Hg densities are $2.10\times10^5$ and $2.05\times10^5$ s$^{-1}$, respectively, and are consistent with the results of McGeoch, Fournier, and Ewart [1].

There is no evidence in Figs. 4 and 10 for more than one exponential term in the rise of the molecular fluorescence intensity. The absence of a term corresponding to the intermediate or the rapid decay terms of the Cd($5\,^3P_1$) state is explained by the fact that these terms correspond to the collisional transfers from the $5\,^3P_1$ state to the $5\,^3P_0$ and $5\,^3P_2$ states [18]. This confirms that the whole Cd $5\,^3P$ manifold (rather than just one state) participates in the formation of the HgCd exciplex, since the time behavior of the $^3P_J$ manifold is dominated by the slowest decay rate.

It is possible to attempt a rough estimate of $k_3$, the three-body rate constant for the production of the HgCd exciplex. The rate of production of HgCd is $\Gamma_a N_a = k_3[\mathrm{Hg}]^2 N_a$. The slowest $\beta_i$, which appears as $\beta$ in Eqs. (8) and (9), is approximately given by $\beta_i = \Gamma_a + \Gamma_c$, where $\Gamma_c$ is a constant term due to the radi-

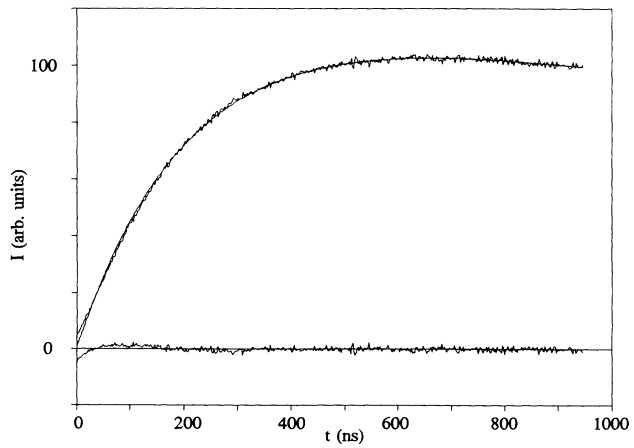


FIG. 6. The rise of the HgCd fluorescence following pump-pulse excitation, corresponding to the first 1-$\mu$s segment of Fig. 4, together with the best fit of Eq. (5) and the residual.

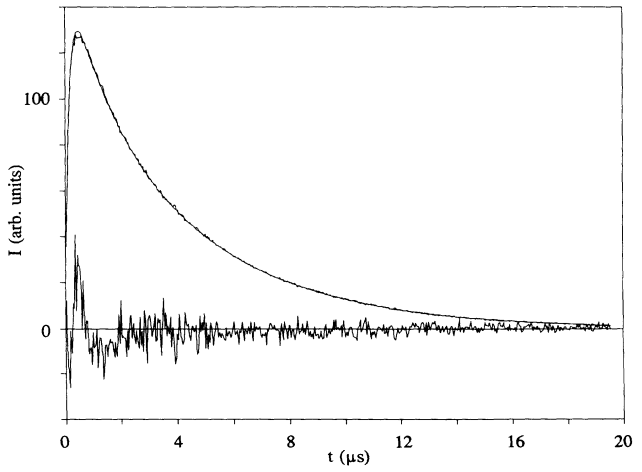


FIG. 7. The best fit of Eq. (8) to the experimental data shown in Fig. 4, together with the residual; the scale of the residual has been magnified by a factor of 10.

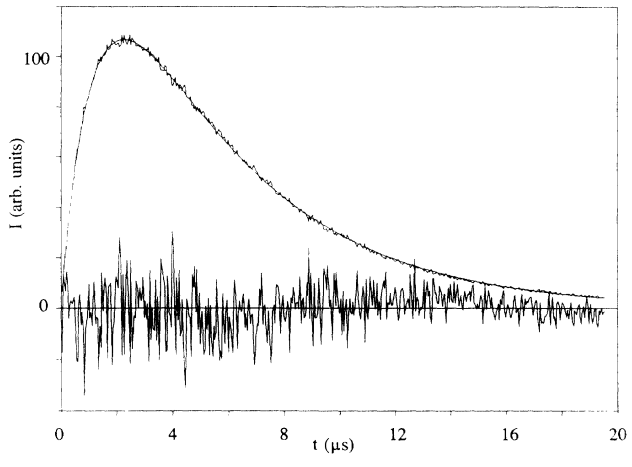


FIG. 8. Time evolution of the 4600-Å HgCd fluorescence band recorded at a Hg density of $1.67\times10^{18}$ cm$^{-3}$, showing the best fit of Eq. (8) and the residual.

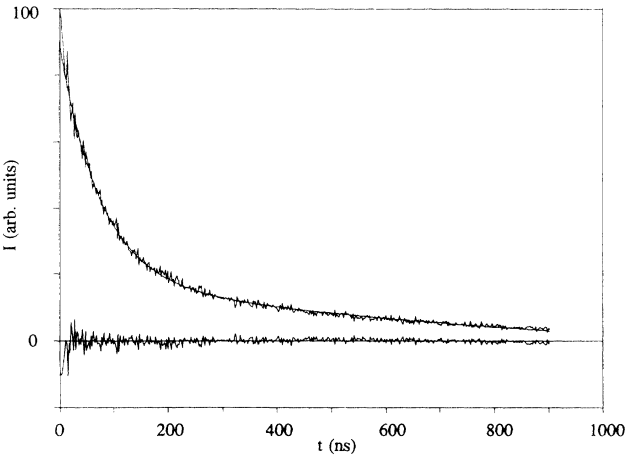


FIG. 9. The decay of the Cd 3261-Å atomic fluorescence following pump-pulse excitation, together with the best fit of Eq. (6) and the residual, recorded at a Hg density of $1.67\times10^{18}$ cm$^{-3}$.

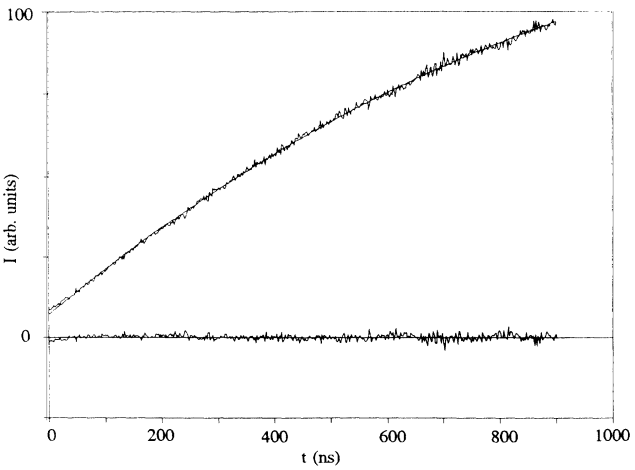


FIG. 10. The rise of the HgCd fluorescence following pump-pulse excitation recorded at the Hg density of $1.67\times10^{18}$ cm$^{-3}$, together with the best fit of Eq. (5) and the residual.

ative decay of the Cd $5\,^3P_1$ state and quenching of the Cd $5\,^3P$ manifold by impurities. Thus $k_3$ can be estimated from the values of $\beta$ and [Hg] at the two temperatures. This procedure yields $k_3 \simeq 2.4\times10^{-31}$ cm$^6$ s$^{-1}$, which is in reasonable agreement with the value found in our study of atomic interactions [18], but is lower than the estimate put forward by McGeoch and co-workers [3,1] by at least a factor of 2.5. These authors reported rise times for the HgCd fluorescence similar to ours, although their Cd densities were about 100 times higher. Some differences in the results are to be expected because of their high Cd density which would cause the pump beam to become rapidly attenuated on resonance and would cause the Cd atoms to be pumped in the wings of the resonance line.

We believe that the observed persistence time of the 4600-Å band is somewhat longer than the radiative lifetimes of the emitting species which are in thermal equilibrium with the metastable $A0^-$ excimers. The analogous spectra of the HgZn excimer [7] and the results of this investigation, which will be discussed below, lead to the conclusion that the $A0^+$ state is not the main carrier of the 4600-Å band and the effective lifetimes of the $A0^+$, $A0^-$, and somewhat higher $A1$ states are determined not only by the radiative lifetimes of the $A0^+$ and $A1$ states, but also by the efficiency of collisional mixing among all three states. These effective lifetimes are always longer than the shortest radiative lifetime, which is probably the radiative lifetime of the state emitting the 4600-Å band. Collisional quenching of the excimer states to the ground state is unlikely because it would require the conversion of a large amount of excitation energy into kinetic energy of relative motion. McGeoch [4] suggested that the $HgCd_2$ trimer, whose PE minimum lies 0.78 eV below the $A0^+$ and $A1$ minima, also participates in the kinetics of the excimer formation, acting as a long-lived reservoir state, and tending to lengthen the effective lifetime of the HgCd excimer. Any substantial contribution arising from trimer-related effects could only occur at much higher Cd densities than that prevalent in our experiment and, accordingly we have not taken into account any formation or decay channels arising from $HgCd_2$ or $Cd_2$ exciplexes.

### B. Pump-and-probe spectroscopy of HgCd

The pump-and-probe experiments revealed the presence of a strong fluorescence spectrum in the 2400–2650-Å region, which could be excited with probe-laser wavelengths ranging from 5600 to 7100 Å. Figure 11 shows traces of the fluorescence bands emitted in bound-free decays of various vibrational levels of a high-lying electronic state to the repulsive part of the ground state. Their intensity profiles represent typical Condon internal diffraction (CID) patterns, which have been described in detail previously [20].

By scanning the pump-probe delay while detecting the CID bands, it is possible to follow the time evolution of the absorbing "reservoir" state. Figures 12(a) and 12(b) show the results of such scans recorded under the same experimental conditions as were employed in producing

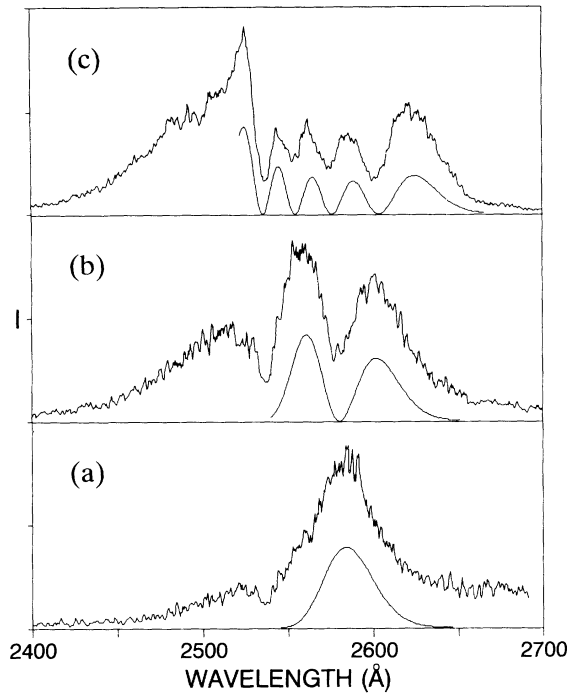


FIG. 11. Traces of fluorescence bands emitted in bound-free decays of $C0^+$ vibronic states of HgCd to the $X0^+$ ground state. The computer-simulated bands are drawn directly under the experimental traces. (a) Emission from the $v'=0$ level, excited with 6729-Å probe radiation corresponding to the $v'=0\leftarrow v''=7$ vibrational component of the $C0^+\leftarrow A0^+$ excitation spectrum; (b) emission from the $v'=1$ level, excited with 6504-Å radiation ($v'=1\leftarrow v''=4$); (c) emission from the $v'=4$ level, excited with 6283-Å radiation ($v'=4\leftarrow v''=2$). The dip in the bands near 2537 Å is due to atomic Hg absorption.

Figs. 4–6 and 8–10, respectively. The corresponding time evolutions are identical within experimental error, confirming that the same HgCd state (or states in thermal equilibrium) are involved in the emission of the 4600-Å band and in the absorption of the probe radiation.

When scanning the probe laser in the 4800–7100-Å region, we observed a structured excitation spectrum which was monitored on various CID peaks and is shown in Fig. 13. At wavelengths beyond 7100 Å the signal faded rapidly and below 5800 Å the spectrum became structureless. The intensity profile of the excitation spectrum suggests that a single, long-lived, lower state was involved in the transitions that were excited with the probe laser. The vibrational components, which are apparent in Fig. 13, belong to both $v'$ and $v''$ progressions. The $v'=0\leftarrow v''=0$ component is not seen in the trace, presumably because of the small Franck-Condon (FC) factor associated with the transition. Information derived from both the excitation spectrum and the fluorescence spectrum led to the positive identification of several $v'$ levels and of 46 peaks, which are labeled in Figs. 11 and 13. Table I lists the vibrational components that were used in the analysis of the spectrum.

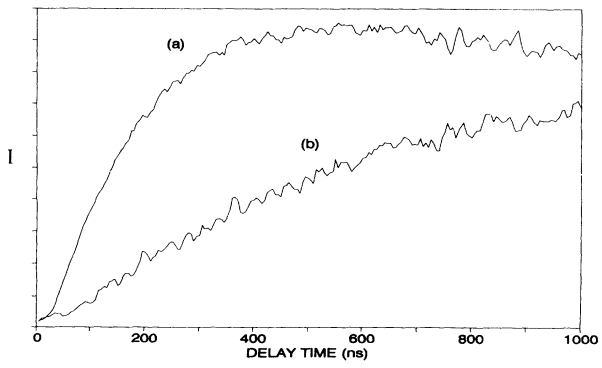


FIG. 12. Plots of the 2460-Å HgCd fluorescence (relative) intensity against pump-probe delay. The plot represents the time evolution of the HgCd reservoir-state population following the pump-laser pulse. (a) Experimental conditions corresponding to those in Fig. 4; (b) conditions as in Fig. 8.

TABLE I. Vibrational components of the $C0^+\leftarrow A0^+$ excitation spectrum. The measured λ (Å) are given in air, the $\tilde{\nu}$ ($cm^{-1}$) are stated *in vacuo*.

| $v'\leftarrow v''$ | λ (Å) | $\tilde{\nu}$ ($cm^{-1}$) |
|---|---|---|
| 0←4 | 6537.5±2.0 | 15 292±5 |
| 0←5 | 6599.5±2.0 | 15 148±5 |
| 0←6 | 6662.5±2.5 | 15 005±6 |
| 0←7 | 6726.0±3.0 | 14 864±7 |
| 0←8 | 6790.0±3.0 | 14 723±7 |
| 0←9 | 6854.5±3.0 | 14 585±7 |
| 0←10 | 6919.5±3.5 | 14 448±8 |
| 0←11 | 6984.8±4.0 | 14 313±8 |
| 1←4 | 6501.8±1.5 | 15 376±4 |
| 1←5 | 6562.9±2.0 | 15 233±5 |
| 1←6 | 6625.0±2.0 | 15 090±5 |
| 1←7 | 6688.0±2.5 | 14 948±6 |
| 1←8 | 6751.0±2.5 | 14 809±6 |
| 2←2 | 6346.8±1.5 | 15 752±4 |
| 2←3 | 6406.8±1.5 | 15 604±4 |
| 2←4 | 6466.5±1.5 | 15 460±4 |
| 2←5 | 6527.2±2.0 | 15 316±5 |
| 3←3 | 6372.9±1.0 | 15 687±3 |
| 3←4 | 6432.5±1.5 | 15 542±4 |
| 3←5 | 6492.5±1.5 | 15 398±4 |
| 4←1 | 6223.9±1.5 | 16 063±4 |
| 4←2 | 6281.8±1.0 | 15 915±4 |
| 4←3 | 6339.8±1.5 | 15 769±4 |
| 4←4 | 6399.0±1.5 | 15 623±4 |
| 5←2 | 6250.2±1.5 | 15 995±4 |
| 5←3 | 6307.0±1.0 | 15 849±3 |
| 6←1 | 6162.7±1.5 | 16 222±4 |
| 6←2 | 6219.0±1.0 | 16 075±3 |
| 6←3 | 6276.5±1.0 | 15 928±3 |
| 7←0 | 6076.8±2.0 | 16 452±6 |
| 7←1 | 6133.0±1.5 | 16 301±4 |
| 7←2 | 6189.0±1.0 | 16 153±3 |
| 7←5 | 6360.8±1.0 | 15 717±3 |
| 8←0 | 6048.3±2.0 | 16 529±6 |
| 8←1 | 6104.0±2.0 | 16 378±6 |
| 9←0 | 6020.4±2.5 | 16 606±7 |
| 10←0 | 5993.3±2.5 | 16 681±7 |
| 11←0 | 5967.0±3.0 | 16 754±9 |

All the prominent components of Fig. 13 that could be clearly assigned were included in a least-squares fit to the expression

$$\tilde{\nu}(v',v'') = T_e + (v'+\tfrac{1}{2})\omega_e' - (v'+\tfrac{1}{2})^2\omega_e'x_e' + (v'+\tfrac{1}{2})^3\omega_e'y_e' - (v''+\tfrac{1}{2})\omega_e'' + (v''+\tfrac{1}{2})^2\omega_e''x_e'' - (v''+\tfrac{1}{2})^3\omega_e''y_e'' , \quad (10)$$

where $\tilde{\nu}(v',v')$ is the wave number ($cm^{-1}$) corresponding to the $v' \leftarrow v''$ transition. The resulting molecular constants are listed in Table II. Since the error in $\omega_e y_e$ is larger than its value, the components were refitted to Eq. (10) without the $\omega_e y_e$ terms. The new constants agreed with those in Table II within the estimated errors. Also, the wave numbers of the components listed in Table I, calculated using the constants determined from the

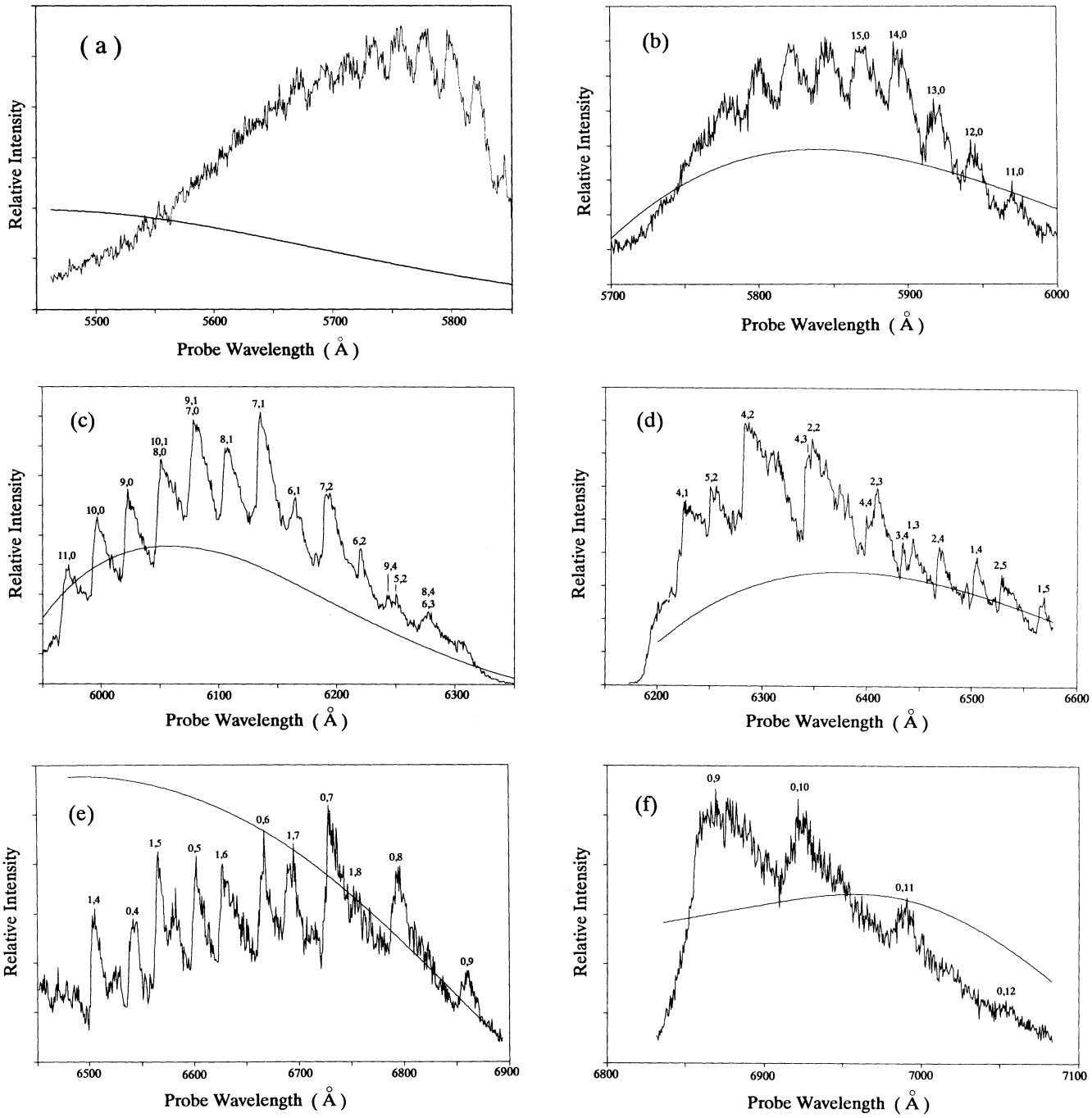


FIG. 13. Traces of the excitation spectrum monitored on various fluorescence peaks of the 2400–2650-Å band; (a) excitation in the 5450–5850-Å range, monitored at 2435 Å, (b) 5700–6000-Å range, monitored at 2650 Å; (c) 5950–6350-Å range, monitored at 2494 Å; (d) 6200–6575-Å range, monitored at 2610 Å; (e) 6500–6880-Å range, monitored at 2585 Å; (f) 6850–7070-Å range, monitored at 2585 Å. The assignments of the vibrational components are shown on the traces; 15,0 stands for $v'=15 \leftarrow v''=0$. The smooth curves indicate the approximate relative output power of the probe laser.

TABLE II. Molecular constants obtained from the fluorescence and excitation spectra. $\Delta r_e$ is listed relative to $r_e(A0^+)$.

| HgCd state | $\omega_e$ ($cm^{-1}$) | $\omega_e x_e$ ($cm^{-1}$) | $\omega_e y_e$ ($cm^{-1}$) | $D_e$ ($cm^{-1}$) | $\Delta r_e$ (Å) |
|---|---|---|---|---|---|
| $X0^+$ | | | | | 1.09±0.08 |
| $A0^+$ | 150.9±0.4 | 0.7±0.1 | 0.0016±0.0050 | 7330±100<br>8132±1160[a] | 0 |
| $C0^+$ | 85.3±0.3 | 0.50±0.06 | 0.0009±0.0030 | 4452±100<br>3638±440[a] | 0.305±0.005[a] |

[a]Assuming the Morse approximation.

analysis, agreed with the measured values within 0.8 $cm^{-1}$, significantly less than the stated experimental errors. Since the Morse potential [21] predicts only terms in $\omega_e x_e$, we believe that it is a reasonably good representation of the lower and upper states, at least close to the PE minima. Table II shows $\Delta r_e = 0.305$ Å, the difference between the equilibrium internuclear separations in the $C0^+$ and $A0^+$ states. This value was yielded by a computer simulation of the vibrational intensity distribution in the excitation spectrum. The simulation was carried out by calculating the Franck-Condon factors for transitions between the $A0^+$ and $C0^+$ vibronic states using $\Delta r_e$ as the adjustable parameter [19].

Figure 11 includes computer-simulated CID fluorescence bands juxtaposed with the experimental traces. In the computer simulation we assumed the Morse potential [21] for the emitting state. The repulsive part of the ground-state PE curve was assumed to have a shape represented by the van der Waals potential,

$$V(r)=\frac{D_e}{n-6}\left\{6\left[\frac{r_0}{r}\right]^n-n\left[\frac{r_0}{r}\right]^6\right\}, \tag{11}$$

where $r_0=r_e''$ is the equilibrium bond length for the ground state. $D_e$, $n$, and $r_0$ were estimated by making certain additional assumptions. The values of $D_e$ and $r_0$ for the ground state of HgCd should lie between the corresponding values for $Hg_2$ and $Cd_2$ [9]. For $Hg_2$, $D_e = 350\pm20$ $cm^{-1}$ and $r_0 = 3.63$ Å [10,22], and for $Cd_2$, $D_e = 323$ $cm^{-1}$ and $r_0$ was estimated to be 4.26 Å [23]. Thus for HgCd we estimate $D_e = 335$ $cm^{-1}$ and $r_0 = 3.95$ Å. Using the van der Waals potential together with the reduced mass of HgCd, it is possible to deduce the vibrational frequency $\omega_e$ for the ground-state potential described by Eq. (11) following an argument similar to that used by Eisel, Zevgolis, and Demtröder [24]. Substituting $n = 7$ in Eq. (11), we obtained $\omega_e = 20.5$ $cm^{-1}$, which lies well between $\omega_e(Hg_2) = 18.5$ $cm^{-1}$ and $\omega_e(Cd_2) = 23$ $cm^{-1}$ [10,23], but $n = 8$ produced $\omega_e(HgCd) = 22$ $cm^{-1}$ and thus it seemed more reasonable to choose $n = 7$ in Eq. (11). The two adjustable parameters that were varied in the course of the computer simulation to obtain the best fit with the intensity distribution in the fluorescence spectrum were $\Delta r_e = r_0 - r_e'$, the difference of the equilibrium internuclear separations in the states associated with the fluorescence emission in the 2400–2650-Å region, and $T_e'$, the energy at the PE minimum of the radiating state relative to the energy of the separated ground-state atoms. The computer-simulation program used the analytical form of the van der Waals ground-state potential to generate the wave functions associated with its energy continuum. They were generated in the JWKB approximation using Langer's condition [25] to obviate problems arising from the singularities in the wave functions at the classical turning points. The products of the upper- and ground-state wave functions were then integrated to produce the simulated intensity profiles of the fluorescence bands. We also assumed the $\nu^3$ dependence of the rate of photon emission (which is equivalent to the photocurrent in the photomultiplier), and no variation of the electronic transition moment with $r$, the internuclear separation [26,27 (pp. 20 and 96)]. The best fit between the experimental and simulated spectra, in terms of the positions of the maxima and minima, was obtained for $r_e''-r_e' = 0.79$ Å, suggesting that $r_e'$, the equilibrium internuclear separation in the emitting state, was $3.95-0.79=3.16$ Å. We do not claim Eq. (11) to represent accurately the whole ground-state PE curve but, in the repulsive region, there is satisfactory agreement between the experimental and simulated spectral intensity profiles. The simulated bands were calculated sufficiently far towards the short wavelengths to incorporate the whole ground-state energy continuum. Simulations assuming $n = 8$ produced similar fits, with the best fit corresponding to $r_e''-r_e' = 0.73$ Å. Since monochromators normally have a pass band with constant $\Delta\lambda$, it might be appropriate to multiply the FC factors by $\nu^5$ rather than $\nu^3$. This changes the relative intensities and shapes of the peaks in the structured continua, but does not change the positions of the maxima and minima which constituted the criterion for best fit.

Bound-free emission bands occasionally include a progression of bound-bound components at the short-wavelength end, which is due to transitions from a rovibrational level of the upper state to various bound levels in the lower state. Sometimes the vibrational structure can be resolved in fluorescence [24], but frequently it remains unresolved, particularly when several rotational levels are excited simultaneously by a broad laser line. The unresolved bound-bound progression tends to have an intensity comparable to that of the bound-continuum band, as is the case, for instance, with the $G0_u^+ \rightarrow X0_g^+$ band in $Hg_2$ [28], where the short-wavelength peak consists of unresolved bound-bound vibrational components which can be simulated since the vibrational constants and the equilibrium internuclear separations for the $G0_u^+$ and $X0_g^+$ states are known [10,22,29]. The analysis of the

short-wavelength peaks of the various bound-continuum fluorescence bands of HgCd, particularly those emitted from higher $v'$ levels, is based on such an interpretation. Even though the equilibrium internuclear separations $r_e''$ and $r_e'$ have not been determined experimentally, we have suggested in Eq. (11) a function for the $X0^+$ ground-state potential, which yields directly the corresponding values for $D_e''$, $r_e''$, and $\omega_e''$. The additional assumption of the Morse potential for the upper state enables us to simulate the intensity profiles of the bound-free fluorescence bands. The simulation clearly indicates that, to obtain the value of $\Delta r_e = r_e'' - r_e'$ consistent with the recorded bands, we must conclude that the transitions take place partly to the bound region of the ground state.

A typical CID pattern (of the "reflection" type), originating from a $v' > 3$ level, is characterized by the presence of two intensity maxima at both ends of the fluorescence band, with a series of weaker maxima between them [30]. Such a band, which was excited with 6136-Å probe radiation, is shown in Fig. 14. The band consists of eight components, though one component is partly obscured by the broadened Hg 2537-Å absorption line. Accordingly, we conclude that the band arises predominantly from the bound-free decay of the $v'=7$ level of the upper state. The experimental trace is drawn in juxtaposition with the simulated bound-free and bound-bound parts of the band. Figure 14(b) shows the short-wavelength end of the band at a somewhat higher resolution, where the agreement between the experimental and simulated bands is even clearer. The relatively intense background in the experimentally recorded trace is ascribed to the low resolution of the monochromator and to the simultaneous excitation (though less efficiently) by the probe radiation of additional $v'$ levels whose fluorescence emission contributes to the background. When using probe radiation at 6079 Å, a wavelength corresponding to a strong excitation component, we recorded a spectrum resulting from the superposition of the $v'=7$ and $v'=9$ CID bands, as confirmed by a simulation of the spectrum.

To assign the particular excitation components to specific $v' \leftarrow v''$ transitions, we used almost the entire structured excitation spectrum over the 5900–6900-Å range. The spacing of the $v''$ levels near the bottom of the potential well of the bound lower state ($v''=0$–$2$) is nearly equal to twice the spacing of the $v'$ levels in the $v'=8$–$10$ region of the upper state and consequently, in the 6000–6100-Å region, the components $v' \leftarrow 0$, $(v'+2) \leftarrow 1$, $(v'+4) \leftarrow 2$, etc., are grouped in tightly packed sequences ($\Delta v'=2$, $\Delta v''=1$). This is illustrated in Fig. 15, which shows a simulated "stick" spectrum and indicates the positions of the excitation components associated with $v''=0,1,2$ levels and various $v'$ levels. The information derived from both excitation and fluorescence spectra leads to the unambiguous assignment of the vibrational components shown in Fig. 15 and thus of all the labeled peaks in the excitation spectrum shown in Figs. 13(b)–13(f). The stick spectrum in Fig. 15 was simulated using $\omega_e' = 85.3\ \text{cm}^{-1}$, $\omega_e' x_e' = 0.5\ \text{cm}^{-1}$, $\omega_e'' = 150.9\ \text{cm}^{-1}$, $x_e'' = 0.7\ \text{cm}^{-1}$, $\Delta r_e = 0.304$ Å, and $T$ (vibrational temperature) $= 650$ K.

Broadening due to the isotope effect is probably the

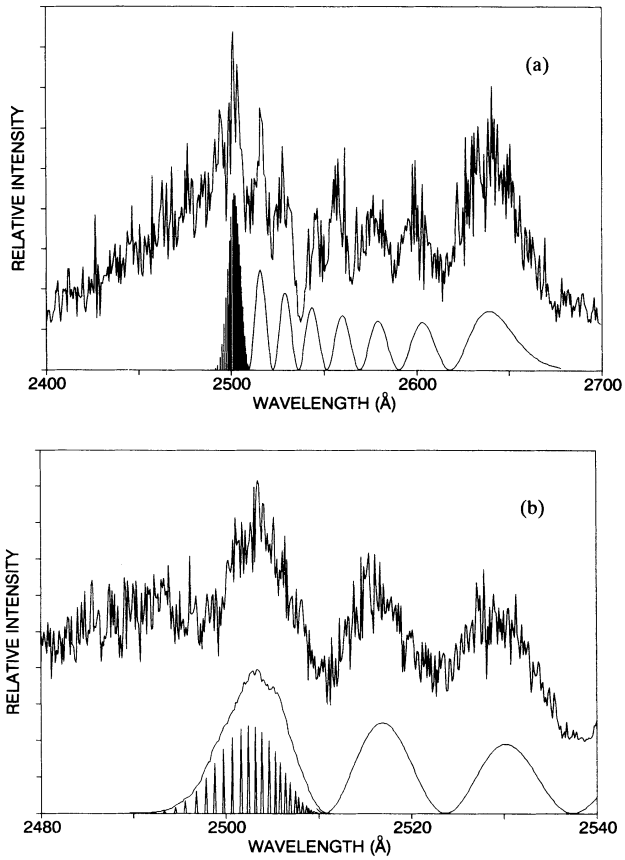


FIG. 14. A trace of the fluorescence band emitted in the decay of the $C0^+$ ($v'=7$) state to the $X0^+$ ground state. The band was excited with 6136-Å probe radiation ($v'=7 \leftarrow v''=1$). The computer-simulated band is drawn under the experimental trace. (b) The short-wavelength part of the band shown at a higher resolution, together with the simulated bound-bound components of the band and the unresolved contour corresponding to the bandwidth of the monochromator.

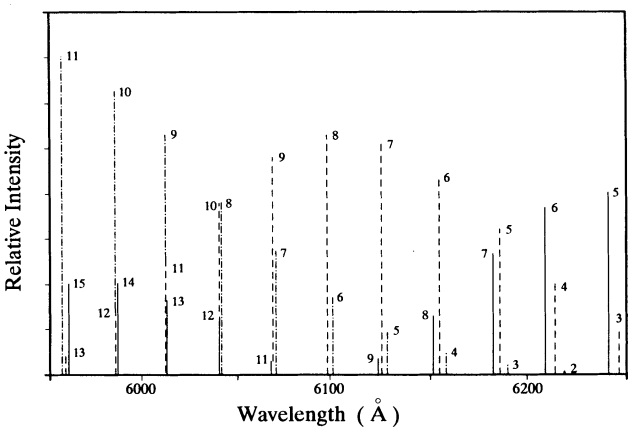


FIG. 15. Computer simulation of a part of the excitation spectrum showing the wavelengths and relative intensities of the vibrational components in the 5960–6260-Å region. $-\cdot-\cdot$, $v' \leftarrow (v''=0)$ transitions, $- - -$, $v' \leftarrow (v''=1)$ transitions; ——, $v' \leftarrow (v''=2)$ transitions. The lengths of all the "sticks" extend from the base line. The numbers in the spectrum represent $v'$ values.

largest factor contributing to the uncertainty in the measured wavelengths of the vibrational components, particularly those associated with large $v'$ or $v''$ quantum numbers. The wave-number separation $\Delta\nu$ between the corresponding vibrational components of two isotopic molecules is given by

$$\Delta\nu=(1-\rho)v'\Delta G_{v'+1/2}-(1-\rho)v''\Delta G_{v''+1/2}$$
$$+(1-\rho)(\omega_e'-\omega_e'')/2\ , \qquad (12)$$

where $v$ is the vibrational quantum number, $\rho=\sqrt{\mu_1/\mu_2}$, $\mu_1$ and $\mu_2$ are the reduced masses of the two isotopic species, and $\Delta G_{v+1/2}$ is the wave-number spacing between the $v$th and $(v+1)$-th vibrational levels in the upper or lower states, respectively [27]. We arrive at the appropriate values of $\mu$ by first calculating a weighted standard deviation $\delta m$ for all the stable isotopes of an element from its average mass, using the known isotopic composition. We then introduce the concept of a "statistically heavy" atom of mass $m_h=m_{\rm av}+\delta m$, and a "statistically light" atom of mass $m_l=m_{\rm av}-\delta m$, leading to a statistically heavy molecule (two "heavy" atoms, $\mu_2$) and a statistically light molecule (two "light" atoms, $\mu_1$). We calculated $\delta m$ to be 1.85 a.u. for Cd and 1.62 a.u. for Hg, which yielded $\mu_1=71.1$ a.u., $\mu_2=73.0$ a.u., and $\rho=0.987$. When substituted in Eq. (12), this gave $\Delta\nu=9$ cm$^{-1}$ or 3.3 Å for the $v'=10\leftarrow v''=0$ component at 5993.2 Å, corresponding to an uncertainty of ±1.6 Å, in agreement with the limit of error stated in Table I. For the $v'=7\leftarrow v''=1$ component at 6133.3 Å, Eq. (12) produced an uncertainty of ±0.9 Å, and for the $v'=0\leftarrow v''=9$ component at 6856 Å, ±3.85 Å, also in agreement with the values in Table I.

Because of the considerable broadening and distortion of the vibrational components in excitation, we had to decide on the definition of a peak position, which is necessary for the quantitative vibrational analysis; we defined the position of a band head consistently for all the observed components as the wavelengh corresponding to 50% local rise in intensity of the leading (short-wavelength) edge of the component, since the rotational structure of the bands was too fine to be resolved [19]. In spite of the consistency, the precision of such definition suffers from a certain arbitrariness of the decision where exactly the 50% rise in intensity is reached, given the level of noise in the spectra. The experimental values given in Table II arise from the natural isotopic combinations, and their errors are actually lower than the differences between the corresponding molecular parameters of the hypothetical "light" and "heavy" molecules. For instance, the values of $\omega_e$ for the two isotopic combinations differ by $(1-\rho)\omega_e$, which is 1.9 cm$^{-1}$ for the lower state (for which the averaged $\omega_e''=150.9$ cm$^{-1}$), which considerably exceeds the 0.4-cm$^{-1}$ uncertainty in the averaged value.

Using the PE function for the ground state described by Eq. (11), the observed fluorescence spectrum leads to the value $T_e'=39\,240\pm100$ cm$^{-1}$ for the PE minimum of the radiating state. We believe this to be the $C0^+$ (Hg $6\,^1S_0$+Cd $5\,^1P_1$) state which, as may be seen in Fig. 1, exhibits an avoided crossing with the $B0^+$ state that causes it to be somewhat shallower than the analogous $C0^+$ state in HgZn [15]. Although the $D1$ state appears in the same general energy region of the PE diagram, there was no evidence of another state being excited by the probe radiation from the reservoir states. The $C0^+$ state corresponds approximately to the $^1\Sigma$ (Hg $6\,^1S$ +Cd $5\,^1P$) state in Hund's case (a), which has a large moment for dipole transitions to the ground state [8]. On the other hand, the $D1$ state derives from the $^3\Pi$ (Hg $6\,^3P$+Cd $5\,^1S$) state, which only decays to the ground state because of the spin-orbit interaction. Even though in the case (c) representation there are avoided crossings between various spin-orbit states correlated to the above asymptotes, the $D1\rightarrow X0^+$ transition appears to be much less probable than the $C0^+\rightarrow X0^+$ transition. If the $D1$ state were the upper state associated with the excitation spectrum, one might expect each vibrational component to be doubled, corresponding to excitation from the $A0^+$ and $A0^-$ states, as was previously observed in the $Hg_2$ excitation spectrum [20]. While the absence of doubling is not conclusive proof since the $A0^+$ and $A0^-$ states might have a very small splitting, it does lend support to the argument that $C0^+$ is the upper state. The lower state associated with the excitation spectrum is most likely the $A0^+$ state, which lies below the $A1$ state and would thus be more highly populated. Such an ordering of the reservoir states would be analogous to that found in $Hg_2$ [19,20] and HgZn [7] where, in each case, $A0^+$ is the lower state connected with excitation bands accompanied by intense singlet-singlet emission spectra.

We have carried out numerous scans of bound-free fluorescence bands, only a few of which are shown in Figs. 11 and 14. On the whole, it was easy to deduce the emitting $v'$ level from the fluorescence spectral profile, consistent with the $v'\leftarrow v''$ assignment in the excitation spectrum. As described above, some of the bands resulted from the decay of two $v'$ levels excited with a particular probe wavelength. The computer simulation of the bands confirmed their interpretation in terms of bound-bound and bound-free transitions. The success of the simulation hinges largely on the correct choice of the ground-state potential. Bearing in mind the various sources of error in the wavelength measurements, including the isotope effect, limited resolution of the monochromator, (unresolved) rotational structure, and the bandwidth of the probe radiation, we assign an uncertainty of ±100 cm$^{-1}$ to our value of 39 240 cm$^{-1}$ for the energy of the $C0^+$ PE minimum, and ±0.07 Å to the value $\Delta r_e=r_e''-r_e'=0.79$ Å. The $C0^+$ state correlates to the (Hg $6\,^1S_0$+Cd $5\,^1P_1$) asymptote, whose energy is 43 692 cm$^{-1}$, and hence $D_e'$ for this state is $43\,692-39\,240=4452\pm100$ cm$^{-1}$. This figure can be compared with the well-depth estimate using the Morse relation $D_e=\omega_e^2/4\omega_e x_e$, which yields $D_e'=3638$ cm$^{-1}$. The $v'=0\leftarrow v''=0$ transition in the $C0^+\leftarrow A0^+$ band is calculated to lie at 6295±2 Å (15 881±5 cm$^{-1}$), which places the bottom of the $A0^+$ potential well at 23 326±100 cm$^{-1}$ above the energy of the ground-state atoms. The $A0^+$ state correlates to the (Hg $6\,^1S_0$+Cd $5\,^3P_1$) asymptote, whose energy is 30 656

$cm^{-1}$, and thus the $A0^+$ well depth is $30\,656 - 23\,326 = 7330 \pm 100$ $cm^{-1}$ while its estimate based on the Morse relation is $D_e'' = 8132$ $cm^{-1}$. The estimates of $D_e'$ and $D_e''$ based on the Morse relation are less accurate than those derived from the modeling analysis, because the use of the Morse relation involves relatively large uncertainties in the $\omega_e x_e$ values and, in any case, the Morse relation does not always yield an accurate $D_e$ value, particularly when the molecular constants are obtained from relatively few vibrational levels located near the bottom of a deep well [27]. Also, $C0^+$ is a perturbed state, which may cause it to conform even less to the Morse potential.

In our analysis we used $r_e = 3.95$ Å for the ground state, from which it follows that $r_e' = 3.16$ Å for the $C0^+$ state and $r_e'' = 2.86$ Å for the $A0^+$ state. This result can be used to suggest that the $A0^+$ state may not be the main carrier of the blue emission band centered at 4600 Å. Since a simple calculation indicates that the ground-state PE curve rises to 2992 $cm^{-1}$ above the atomic asymptote at $r = 2.86$ Å, the photon energy of the $A0^+$ $(v=0) \rightarrow X0^+$ emission would be expected to be $23\,326 - 2992 = 20\,334$ $cm^{-1}$, which is equivalent to about 4917 Å in terms of photon wavelength. The transient population of the $A0^+$ state would be expected to have a Boltzmann-type quasiequilibrium vibrational distribution, but it can be shown [31] that the emission band from the upper state should still be centered at the wavelength corresponding to the emission from the $v=0$ state, unless the transition moment varied dramatically with $r$. Changing the ground-state potential parameter from $n=7$ to $n=8$ did not alter this conclusion after incorporating the revised $\Delta r_e$ between the $C0^+$ and $X0^+$ states to model the structured $C0^+ \rightarrow X0^+$ fluorescence bands. It would accordingly seem that the higher-lying Al (Hg $6\,^1S_0$ + Cd $5\,^3P_1$) state is the main emitting state of the 4600-Å fluorescence.

To verify this conclusion, we carried out a FC simulation of the 4600-Å band, assuming it to be emitted by the $A0^+$ state. The vibrational wave functions for the $v'$ states were written on the basis of the Morse potential and the spectroscopic constants given in Table II, and the ground state was represented by Eq. (11). The simulation was done following the procedure outlined by Bender *et al.* [31], with the intensity distribution given by

$$I(\nu) \sim \left| \int_0^\infty \Psi_u(v',r)\Psi_g(E_g,r)dr \right|^2 \nu^6 , \qquad (13)$$

since the experimental band intensity was stated in relative units of (intensity)/$\Delta\lambda$ [32]. In Eq. (13), $\nu = E_{v'} - E_g$ ($cm^{-1}$) is the frequency of the emitted radiation, $E_{v'}$ is the total energy of the vibrational level $v'$, and $E_g$ is the (nonquantized) energy of the ground-state quasimolecule, resulting from the radiative decay. This model does not take into account rotational effects, which would only very slightly affect the overall result [33], and assumes that the electronic transition moment remains constant over the relatively small range of $r$, the internuclear separation. The simulated profile is included in Fig. 3 and consists of contributions from the 16 lowest $v'$ levels of the $A0^+$ state, which was assumed to have a Boltzmann population distribution. The slight wiggles on the short-wavelength wing of the envelope are due to the fact that not all the $v'$ levels were included in the simulation, nor was the rotational structure; similar effects have been observed by Bender *et al.* [31]. It may be seen that the simulated band reproduces quite well the overall profile of the experimental trace, but is clearly shifted by about 160 Å towards longer wavelengths. This shift of about 730 $cm^{-1}$ corroborates the conclusion reached from the bound-continuum band fluorescence, that $A0^+$ is not the main emitting source of the 4600-Å, band, which is mainly due to a higher state having higher transition probabilities, which could only be the $A1$ state. The 730-$cm^{-1}$ splitting between the $A0^+$ and $A1$ states appears to be reasonable, assuming that the equilibrium internuclear separations in the two states are similar. In the similar HgZn exciplex the $A0^+$-$A1$ energy splitting was found to be 940 $cm^{-1}$ [7].

To ensure that the observed bands were indeed due to HgCd, we carried out a supplementary experiment in which we subjected a quartz cell, filled with pure Cd vapor, to pump-and-probe irradiation under identical conditions as those described above. When irradiated with 3261-Å pulses, the vapor emitted faint fluorescence near 4000 Å which had a persistence time of less than 100 ns. We did not attempt to analyze this emission, which might be due to CdH, by analogy with the ZnH fluorescence [34], which was observed even when efforts were made to exclude $H_2$ from the system. We also detected the Cd atomic resonance fluorescence which exhibited a much longer effective lifetime (1.5–2.0 $\mu$s) than was observed in the HgCd vapor mixture. When pump-and-probe excitation was employed, no signal was detected in the 2400–2600-Å region. The results of this experiment indicate that the exciplex fluorescence and excitation bands observed in the Hg-Cd vapor mixture were due to HgCd.

## V. SUMMARY AND CONCLUSIONS

Fluorescence and excitation spectra of the HgCd exciplex were produced by irradiating a Hg-Cd vapor mixture in a quartz cell, using one- and two-step laser excitation. When the vapor mixture was pumped with 3261-Å radiation corresponding to the Cd $5\,^3P_1 \leftarrow 5\,^1S_0$ transition, the $5\,^3P_0$ and $5\,^3P_2$ states also participated in the formation of the HgCd exciplex by three-body collisions, a process for which the rate coefficient was estimated to be $2.4 \times 10^{-31}$ $cm^6 s^{-1}$, in good agreement with the more accurate value found in another experiment [18]. Of the three low-lying excimer states, the $A0^+$ and $A1$ states can decay to the $X0^+$ ground state and the $A0^-$ state is metastable, though all three states are collisionally mixed and decay with a common effective decay rate. Analysis of the fluorescence and excitation bands yielded the spectroscopic constants for the $C0^+$ and $A0^+$ states. A

semiempirical model for the $X0^+$ ground state is suggested to account for the intensity profiles of the $C0^+ \rightarrow X0^+$ bound-free fluorescence bands. The molecular constants derived from the experimental data are collected in Table II.

ACKNOWLEDGMENTS

This research was supported by the Canadian Department of Defence and by the Natural Sciences and Engineering Research Council of Canada.

[1] M. W. McGeoch, G. R. Fournier, and P. Ewart, J. Phys. B **9**, L121 (1976).
[2] G. R. Fournier and M. W. McGeoch, J. Appl. Phys. **49**, 2651 (1978).
[3] M. W. McGeoch and G. R. Fournier, J. Appl. Phys. **49**, 2659 (1978).
[4] M. W. McGeoch, J. Chem. Phys. **72**, 140 (1980); **73**, 2534 (1980).
[5] A. Mandl, M. Kovacs, B. Srivastava, J. H. Jacob, and D. Klimek, Phys. Rev. A **24**, 3160 (1981).
[6] J. B. West, H. Komine, and E. A. Stappaerts, J. Appl. Phys. **50**, 7929 (1979).
[7] L. Krause, J. B. Atkinson, and W. E. Baylis, University of Windsor Final Technical Report on Contract No. W7701-0-2313/01-XSK (National Defence), 1993 (unpublished); J. Supronowicz, E. Hegazi, J. B. Atkinson, and L. Krause, Chem. Phys. Lett. **218**, 240 (1994); **222**, 149 (1994).
[8] J. Sienkiewicz (private communication); see also E. Czuchaj, F. Rebentrost, H. Stoll, and H. Preuss, Chem. Phys. Lett. **197**, 187 (1992).
[9] J. O. Hirschfelder, C. F. Curtiss, and R. B. Bird, *Molecular Theory of Gases and Liquids* (Wiley, New York, 1954), p. 222.
[10] R. D. van Zee, S. C. Blankespoor, and T. S. Zwier, J. Chem. Phys. **88**, 4650 (1988).
[11] M. Czajkowski, R. Bobkowski, and L. Krause, Phys. Rev. A **40**, 4338 (1989).
[12] B. Huron, J. P. Malrien, and P. J. Rancurel, J. Chem. Phys. **58**, 5745 (1973).
[13] P. J. Hay, T. H. Dunning, and R. C. Raffenetti, J. Chem. Phys. **65**, 2679 (1976).
[14] T. L. Hill, *Introduction to Statistical Thermodynamics* (Addison Wesley, Reading, MA, 1960), Chap. 20.
[15] J. Supronowicz, E. Hegazi, J. B. Atkinson, and L. Krause, Phys. Rev. A **37**, 3818 (1988).
[16] J. G. Eden, Opt. Commun. **25**, 201 (1978).
[17] G. R. Fournier, J. Chem. Phys. **91**, 1548 (1989).
[18] J. Supronowicz, M. J. Hinek, J. B. Atkinson, and L. Krause, Chem. Phys. Lett. **213**, 282 (1993).
[19] R. J. Niefer, J. Supronowicz, J. B. Atkinson, and L. Krause, Phys. Rev. A **35**, 4629 (1987).
[20] R. J. Niefer, J. Supronowicz, J. B. Atkinson, and L. Krause, Phys. Rev. A **34**, 1137 (1986).
[21] P. M. Morse, Phys. Rev. **34**, 57 (1929).
[22] A. Zehnacker, M. C. Duval, C. Jouvet, C. Lardeux-Dedonder, D. Solgadi, B. Soep, and D. Benoist d'Azy, J. Chem. Phys. **86**, 6565 (1987).
[23] M. Czajkowski, R. Bobkowski, and L. Krause, Phys. Rev. A **41**, 277 (1990).
[24] D. Eisel, D. Zevgolis, and W. Demtröder, J. Chem. Phys. **71**, 2005 (1979).
[25] P. E. Langer, Phys. Rev. **51**, 669 (1937).
[26] R. S. Mulliken, J. Chem. Phys. **55**, 309 (1971).
[27] G. Herzberg, *Spectra of Diatomic Molecules* (van Nostrand, New York, 1950).
[28] J. Supronowicz, R. J. Niefer, J. B. Atkinson, and L. Krause, J. Phys. B **19**, 1153 (1986); J. Supronowicz, W. Kedzierski, J. B. Atkinson, and L. Krause (unpublished).
[29] W. Kedzierski, J. Supronowicz, A. Czajkowski, M. J. Hinek, J. B. Atkinson, and L. Krause, Chem. Phys. Lett. **218**, 314 (1994).
[30] See, for instance, J. Tellinghuisen, J. Mol. Spectrosc. **103**, 455 (1984).
[31] C. F. Bender, T. N. Rescigno, H. F. Schaefer, and A. E. Orel, J. Chem. Phys. **71**, 1122 (1979).
[32] See, for example, M. Masters, J. Huennekens, W.-T. Luh, L. Li, A. M. Lyyra, K. Sando, V. Zafiropulos, and W. C. Stwalley, J. Chem. Phys. **92**, 5801 (1990).
[33] G. Rodriguez and J. G. Eden, J. Chem. Phys. **95**, 5539 (1991).
[34] W. Kedzierski, J. Supronowicz, J. B. Atkinson, and L. Krause, Can. J. Phys. **28**, 526 (1990).